Electronic supplementary information for

A two-dimensional covalent organic framework with single-atom manganese for electrochemical NO reduction: a computational study

Jing Yu,[†] Yu Wang,[†,*] Yafei Li[†,*]

[†]Jiangsu Key Laboratory of New Power Batteries, Jiangsu Collaborative Innovation Centre of Biomedical Functional Materials, School of Chemistry and Materials Science, Nanjing Normal University, Nanjing 210023, P. R. China.

To whom correspondence should be addressed. E-mail: yu.wang@njnu.edu.cn(YW) and liyafei@njnu.edu.cn(YL)

Computational methods

All calculations were performed by using density functional theory (DFT) as implemented in the Vienna ab initio simulation package (VASP).[1,2] The exchange-correlation potential was treated by generalized gradient approximation (GGA) in the form of Perdew−Burke−Ernzerhof (PBE), and the projector-augmented wave approach was adopted.[3,4,5] The kinetic energy cutoff was set to 400 eV after a series of tests. The energy convergence criterion is set to 5×10^{-5} eV. The Brillouin zone integration was conducted by using a 2 × 2 × 1 k-point mesh. The DFT-D3 method was adopted to describe van der Waals interactions.[6] A vacuum layer in the z-direction is set to over 20 Å. Spin polarization was considered throughout the calculations. Previous studies showed that PBE functional can sufficiently describe the electronic and adsorption properties of various types of single-atom catalysts with the Metal-N_4 moiety;[7,8] considering the large size of each COF nanosheet (77 atoms per unit cell), the high-cost hybrid functional calculations were not performed in this work.

On the basis of the computational hydrogen electrode mode[9], we evaluated the change in the Gibbs free energy (ΔG) for each elemental step according to the following expression:

$$\Delta G = \Delta E_{DFT} + \Delta E_{ZPE} - T\Delta S - \Delta G_U + \Delta G_{pH} \quad (1)$$

where ΔE_{DFT} is the DFT-computed electronic energy difference, ΔE_{ZPE} is the change in zero-point energy, and $T\Delta S$ is the entropy change at 298 K. The entropies of the free molecules (NO, H_2, N_2O, and NH_3) are obtained from the NIST database.[10] $\Delta G_U = -eU$ is the free energy contribution introduced by the electrode potential U. ΔG_{pH} is the correction of pH (taken as 1), which can be defined as $\Delta G_{pH} = k_B T \times pH \times \ln 10$.

The energy barriers of the elementary reaction steps were calculated by using the climbing-image nudged elastic band (CI-NEB) method.[11] We constructed a 2 H_2O model to describe the solvation effect.[12] Moreover, the Poisson–Boltzmann implicit solvation model was used to establish the relationships between the extra electrons and electrode potentials, and it takes advantage of the fact that the electrostatic potential goes to zero in the electrolyte region.[13,14] The cavity setting in VASP-sol was turned off to avoid numerical instabilities. For each reaction species, independent

calculations with five different system charges were performed. For a charged slab, the potential with respect to standard hydrogen electrode (SHE) was calculated by:

For a charged slab, the potential with respect to standard hydrogen electrode (SHE) was calculated by:

$$U = W_f/e - 4.60 \quad (2)$$

where U is electrode potential, W_f is the work function, and 4.60 is the predicted standard hydrogen electrode scale based on VASPsol calculations.[13,14] The work function can be controlled by adjusting the number of charges. The values of U_{SHE} were further regulated to the reversible hydrogen electrode (RHE) scale by a potential shift of 0.0592 × pH, where the value of pH was set as 1 in the work. The potential-dependent energy can be calculated by:[15,16]

$$E_{free}(U) = E_{DFT} + \int_0^q < \overline{V_{TOT}} > dQ + qW_f \quad (3)$$

For each species, we can deduce the energy at a given potential by fitting the five energy-potential points in a quadratic form.

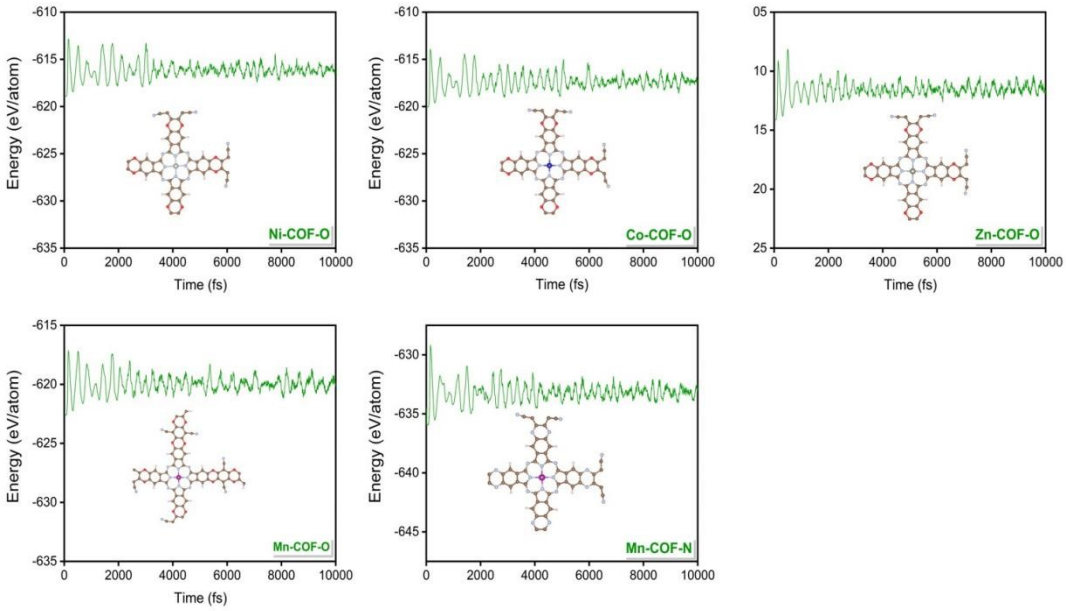

Fig. S1 Evolution of the total energy of ab initio molecular dynamics (AIMD) simulation for M-COF@O (M= Ni, Co, Zn, Mn) and Mn-COF@N at 300 K. The inset is the snapshot of the structure at 10 ps.

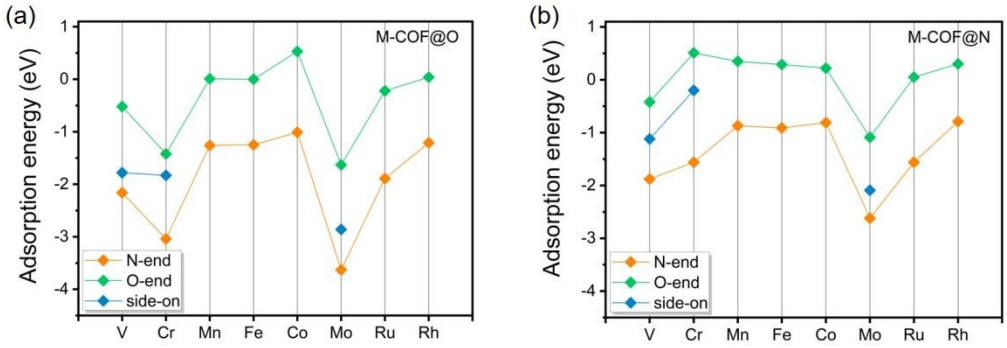

Fig. S2 Adsorption energies of NO on (a) M-COF@O and (b) on M-COF@N with N-end, O-end, and side-on patterns.

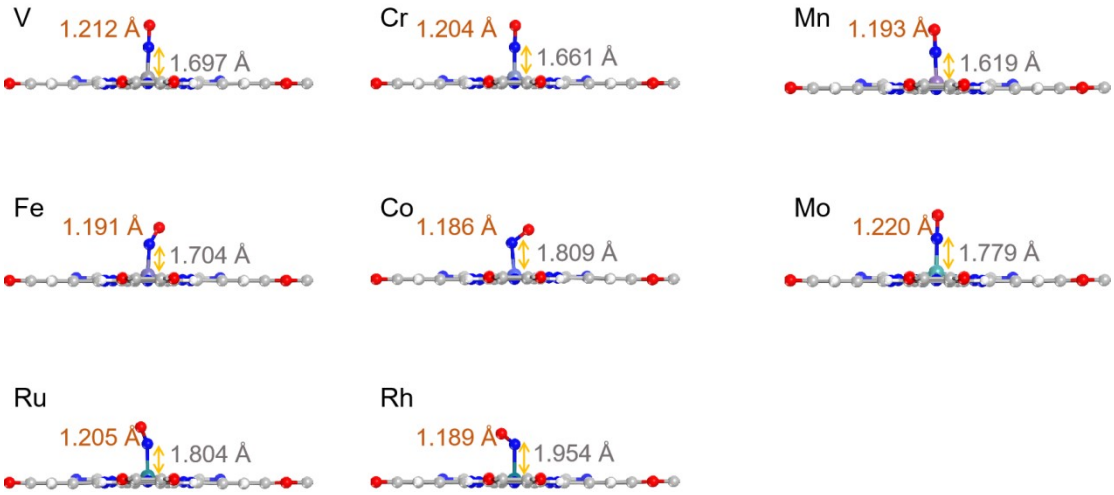

Fig. S3 The N-O bond length and N-M bond length of adsorbed NO on M-COF@O (M = V, Cr, Mn, Fe, Co, Mo, Ru and Rh).

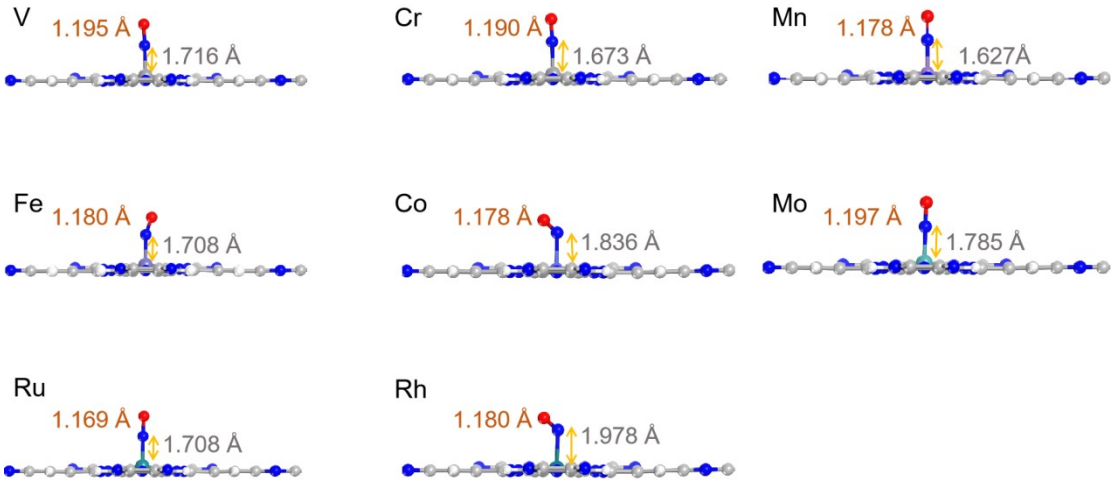

Fig. S4 The N-O bond length and N-M bond length of adsorbed NO on M-COF@N (M = V, Cr, Mn, Fe, Co, Mo, Ru and Rh).

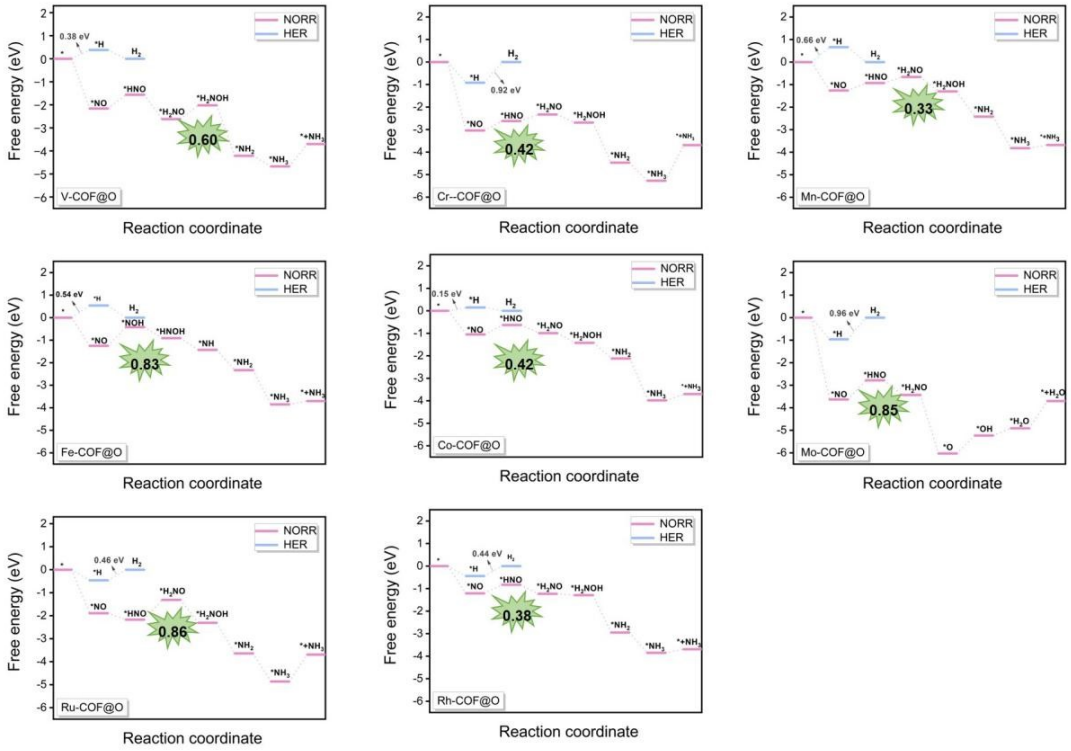

Fig. S5 Free energy diagrams via the most favorable pathway for M-COF@O (M = V, Cr, Mn, Fe, Co, Mo, Ru and Rh).

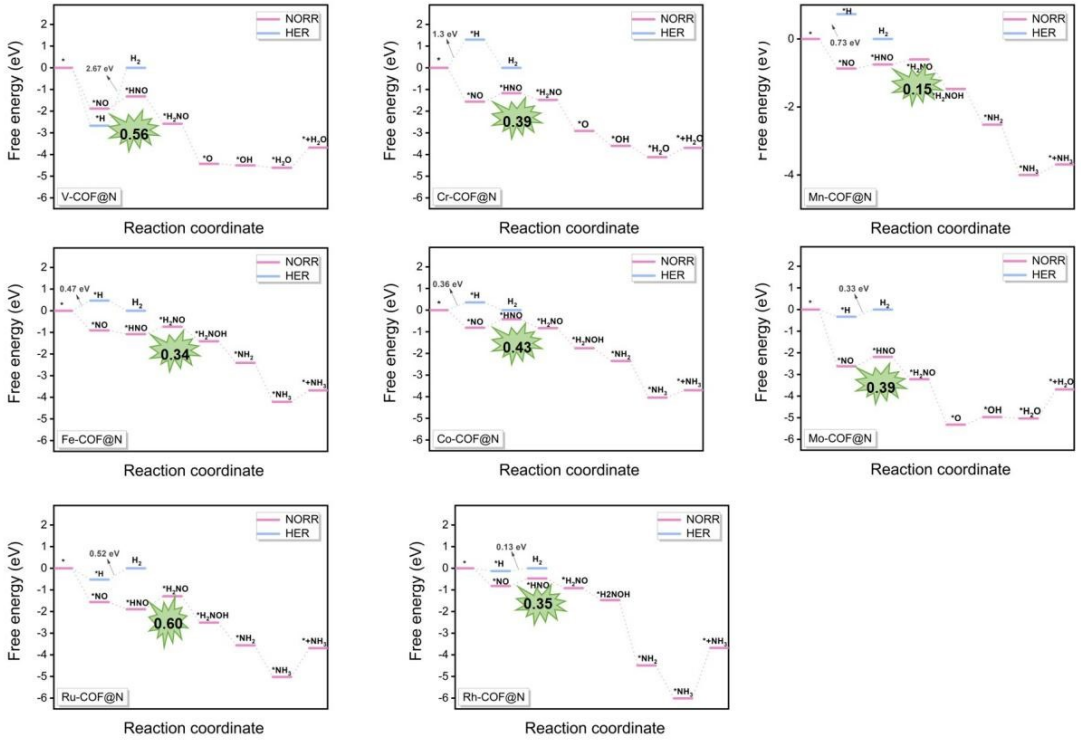

Fig. S6 Free energy diagrams via the most favorable pathway for M-COF@N (M = V, Cr, Mn, Fe, Co, Mo, Ru and Rh).

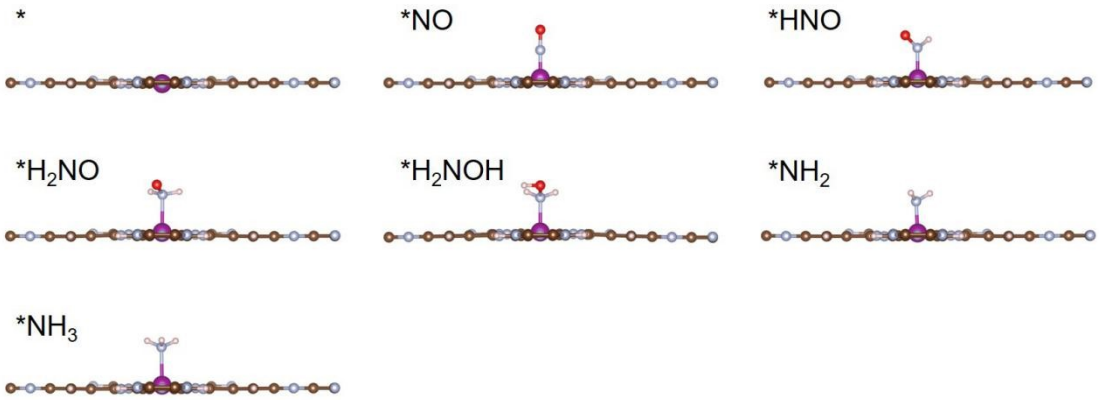

Fig. S7 Side views of NORR intermediates of Mn-COF@N

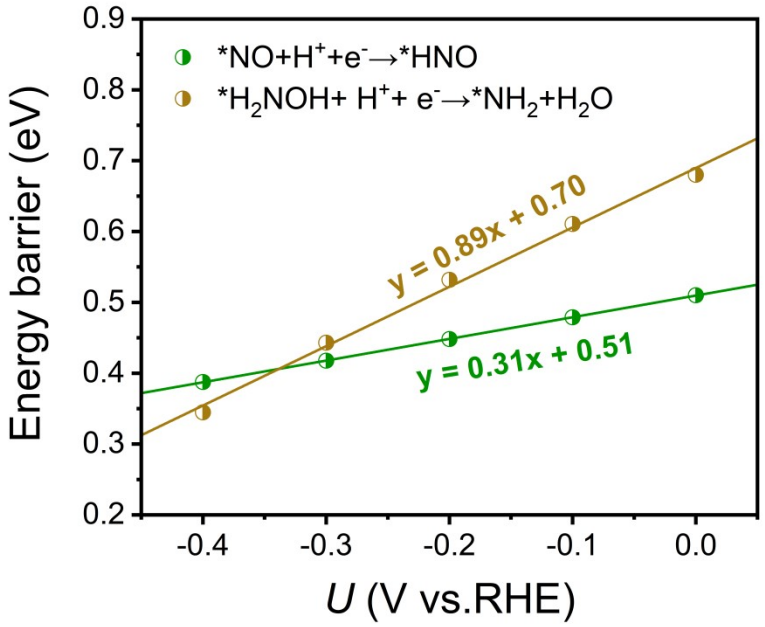

Fig. S8 The kinetic barriers as a function of potential of (a) *NO to *HNO (b) *H_2NOH to *NH_2 on Mn-COF@N.

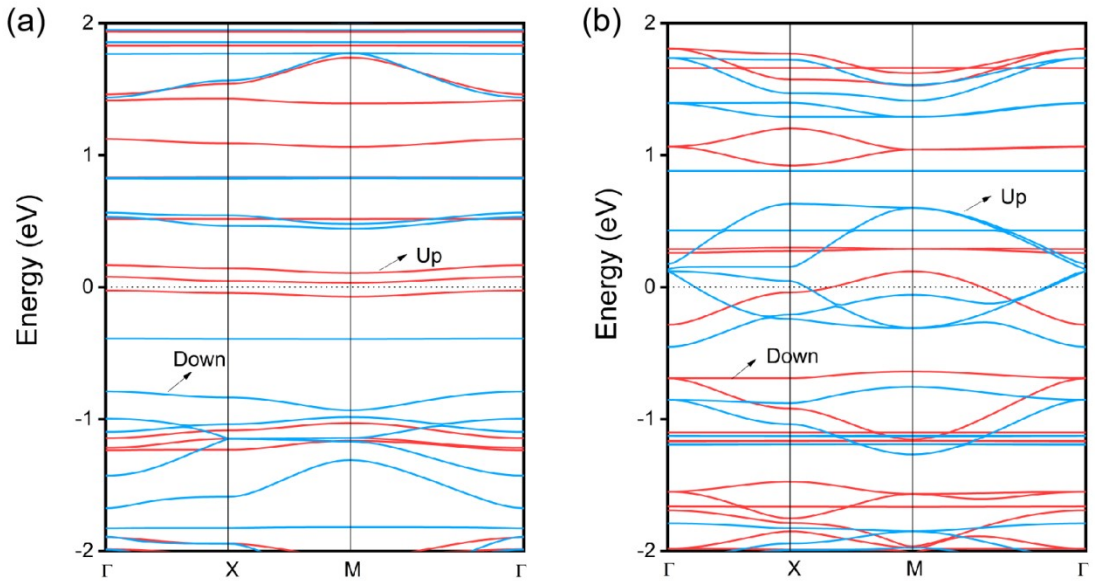

Fig. S9 (a) Band structure of Mn-COF@O and (b) of Mn-COF@N.

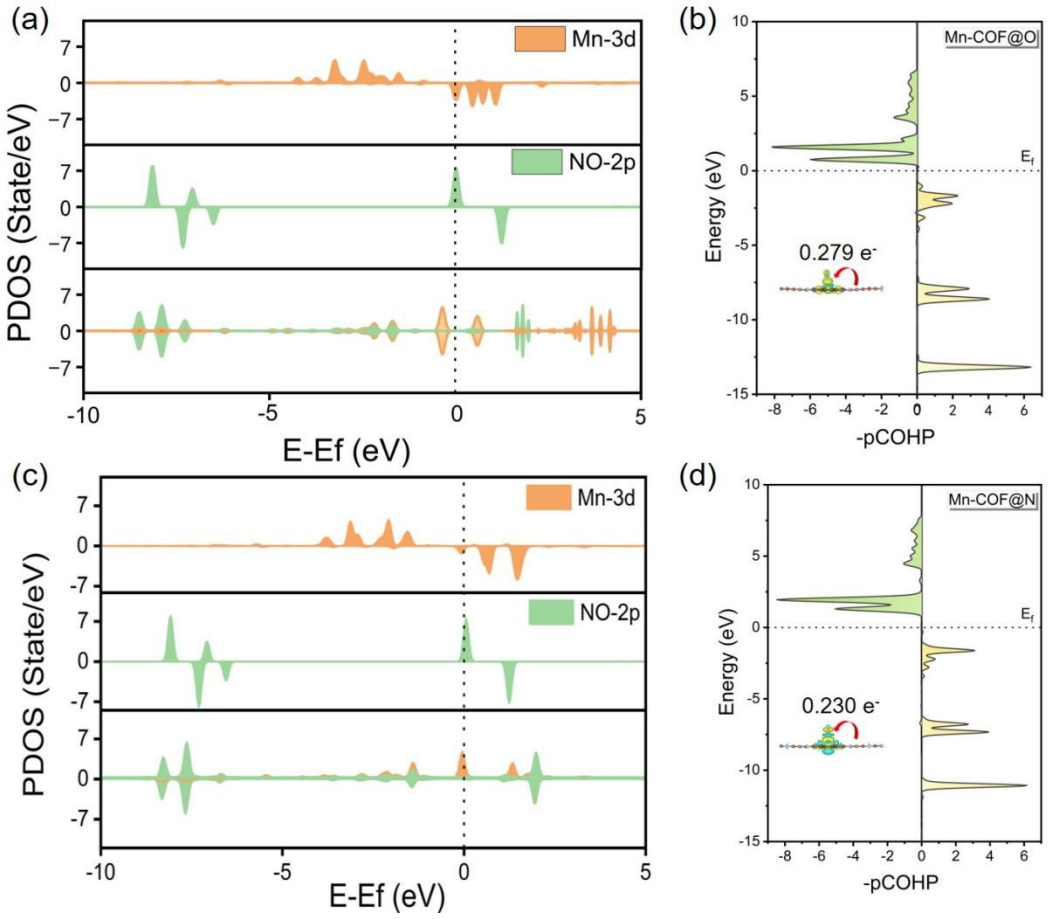

Fig. S10 (a, c) Partial density of states (PDOS) of the Mn-3d orbitals of the adsorbate-free COF slab, the 2p orbitals of free NO molecule, and the Mn-3d and NO-2p orbitals of *NO: (a) Mn-COF@O and (c) Mn-COF@N. The Fermi level is set to be 0 eV. (b, d) Projected crystal orbital Hamilton population (-pCOHP) for NO adsorbed on (b) Mn-COF@O and (d) Mn-COF@N. The inserts are charge density differences. The iso-surface value is 0.0018 e $Å^{-3}$, and the electron depletion and accumulation regions are shown in green and yellow, respectively.

Table S1. The number of electrons (*N*e) involved in the dissolution for the bulk metals, standard dissolution potentials U°_{diss}(metal,bulk), total energy of metal atoms in their bulk phase (E_{TM}), formation energy (E_f) , and computed dissolution potentials (U_{diss}) of M-COF@O.

Metal	*N*e	U°_{diss}(metal,bulk) (V)	E_{TM} (eV)	E_f (eV)	U_{diss} (V)
V	2	-1.18	-9.09	-4.54	1.09
Cr	2	-0.91	-9.64	-5.67	1.92
Mn	2	-1.19	-9.16	-5.46	1.54
Fe	2	-0.45	-8.46	-4.90	2.00
Co	2	-0.28	-7.11	-4.97	2.21
Ni	2	-0.26	-5.78	-5.18	2.33
Cu	2	0.34	-4.10	-3.76	2.22
Zn	2	-0.76	-1.27	-4.90	1.69
Nb	3	-1.10	-10.11	-3.17	-0.04
Mo	3	-0.20	-10.86	-3.26	0.89
Ru	2	0.46	-9.28	-3.49	2.21
Rh	2	0.60	-7.36	-4.41	2.80

Table S2. The number of electrons (*Ne*) involved in the dissolution for the bulk metals, standard dissolution potentials U°_{diss}(metal,bulk), total energy of metal atoms in their bulk phase (E_{TM}), formation energy (E_f) , and computed dissolution potentials (U_{diss}) of M-COF@N.

Metal	Ne	U_{diss}°(metal,bulk) (V)	E_{TM} (eV)	E_f (eV)	U_{diss} (V)
V	2	-1.18	-9.09	-4.50	1.07
Cr	2	-0.91	-9.64	-4.90	1.54
Mn	2	-1.19	-9.16	-4.85	1.23
Fe	2	-0.45	-8.46	-4.25	1.68
Co	2	-0.28	-7.11	-5.81	2.62
Ni	2	-0.26	-5.78	-4.35	1.92
Cu	2	0.34	-4.10	-2.94	1.81
Zn	2	-0.76	-1.27	-4.08	1.28
Nb	3	-1.10	-10.11	-2.78	-0.17
Mo	3	-0.20	-10.86	-2.63	0.68
Ru	2	0.46	-9.28	-3.16	2.04
Rh	2	0.60	-7.36	-4.19	2.69

Table S3. Adsorption energies of NO on M-COF@O with N-end ($\Delta G_{N\text{-}end}$), O-end ($\Delta G_{O\text{-}end}$), and side-on patterns ($\Delta G_{side\text{-}on}$).

Metal	$\Delta G_{N\text{-}end}$ (eV)	$\Delta G_{O\text{-}end}$ (eV)	$\Delta G_{side\text{-}on}$ (eV)
V	-2.16	-0.52	-1.78
Cr	-3.04	-1.42	-1.83
Mn	-1.26	0.01	N.A.
Fe	-1.25	0.00	N.A.
Co	-1.01	0.53	-1.08
Mo	-3.63	-1.63	-2.86
Ru	-1.89	-0.22	N.A.
Rh	-1.21	0.04	N.A.

Table S4. Adsorption energies of NO on M-COF@N with N-end ($\Delta G_{\text{N-end}}$), O-end ($\Delta G_{\text{O-end}}$), and side-on patterns ($\Delta G_{\text{side-on}}$).

Metal	$\Delta G_{\text{N-end}}$ (eV)	$\Delta G_{\text{O-end}}$ (eV)	$\Delta G_{\text{side-on}}$ (eV)
V	-1.88	-0.42	-1.12
Cr	-1.56	0.51	-0.20
Mn	-0.87	0.35	N.A.
Fe	-0.91	0.29	N.A.
Co	-0.81	0.22	N.A.
Mo	-2.62	-1.09	-2.09
Ru	-1.56	0.05	N.A.
Rh	-0.79	0.30	N.A.

Table S5. The N–O bond length (Å) of adsorbed NO on M-COF@O and M-COF@N (M = V, Cr, Mn, Fe, Co, Mo, Ru and Rh).

Metal	N–O bond length for M-COF@O (Å)	N–O bond length for M-COF@N (Å)
V	1.212	1.195
Cr	1.204	1.190
Mn	1.193	1.178
Fe	1.191	1.180
Co	1.186	1.178
Mo	1.220	1.197
Ru	1.205	1.169
Rh	1.189	1.180

Table S6. The charge of *NO of M-COF@O and M-COF@N (M = V, Cr, Mn, Fe, Co, Mo, Ru and Rh) based on the Bader charge analysis.

Metal	Charge for M-COF@O (*e*)	Charge for M-COF@N (*e*)
V	0.491	0.440
Cr	0.399	0.380
Mn	0.279	0.230
Fe	0.293	0.116
Co	0.209	0.112
Ni	0.204	−0.058
Cu	−0.034	−0.183
Zn	−0.007	−0.160
Mo	0.670	0.440
Ru	0.294	0.108
Rh	0.186	0.099
Pd	0.156	−0.119
Ag	0.200	−0.159

References

[1] G. Kresse and J. *Furthmuller, Phys. Rev. B*, 1996, **54**, 11169−11186.

[2] G. Kresse and D. Joubert, *Phys. Rev. B*, 1999, **59**, 1758−1775.

[3] J. P. Perdew, K. Burke and M. Ernzerhof, *Phys. Rev. Lett.*, 1996, **77**, 3865.

[4] P. E. Blöchl, *Phys. Rev. B*, 1994, **50**, 17953−17979.

[5] J. P. Perdew, J. A. Chevary, S. H. Vosko, K. A. Jackson, M. R. Pederson, D. J. Singh and C. Fiolhais, *Phys. Rev. B*, 1992, **46**, 6671−6687.

[6] S. Grimme, *J. Comput. Chem.*, 2006, **27**, 1787.

[7] X. Yao, L. Huang, E. Halpren, L. Chen, Z. Chen and C. V. Singh, *J. Am. Chem. Soc.*, 2023, **145**, 26249–26256.

[8] Y. Wang, Y-J. Tang and K. Zhou, *J. Am. Chem. Soc.,* 2019, **141**, 14115–14119.

[9] J. K. Norskov, J. Rossmeisl,A. Logadottir, L. Lindqvist, J. R. Kitchin,T. Bligaard and H. Jonsson, *J. Phys. Chem. B*, 2004, **108**, 17886−17892.

[10] Computational Chemistry Comparison and Benchmark Database.

[11] G. Henkelman, B. P. Uberuaga and H. Jónsson, *J. Chem. Phys.*, 2000, **113**, 9901–9904.

[12] Y. Wang, Y.-J. Tang and K. Zhou, *J. Am. Chem. Soc.,* 2019*,* **141***,* 14115–14119.

[13] K.Mathew,R. Sundararaman, K. Letchworth-Weaver, T. Arias and R. G. Hennig, *J. Chem. Phys.*, 2014, **140**, 084106.

[14] K. Mathew, V. C. Kolluru, S. Mula, S. N. Steinmann and R. G. Hennig, *J. Chem. Phys.*, 2019, **151**, 234101.

[15] J. S. Filhol and M. Neurock, *Angew. Chem. Int. Ed.*, 2006, **118**, 416−420.

[16] Y. Wang, T. Liu and Y. Li, *Chem. Sci.*, 2022, **13**, 6366-6372